

Magnetic helicity and the evolution of decaying magnetohydrodynamic turbulence

Arjun Berera* and Moritz Linkmann†

SUPA, School of Physics and Astronomy, University of Edinburgh, Mayfield Road, EH9 3JZ, UK

Ensemble averaged high resolution direct numerical simulations of reverse spectral transfer are presented, extending on the many single realization numerical studies done up to now. This identifies this type of spectral transfer as a statistical property of magnetohydrodynamic turbulence and thus permits reliable numerical exploration of its dynamics. The magnetic energy decay exponent from these ensemble runs has been determined to be $n_E = (0.47 \pm 0.03) + (13.9 \pm 0.8)/R_\lambda$ for initially helical magnetic fields. We show for the first time that even after removing the Lorentz force term in the momentum equation, thus decoupling it from the induction equation, reverse spectral transfer still persists. The induction equation is now linear with an externally imposed velocity field, thus amenable to numerous analysis techniques. A new door has opened for analyzing reverse spectral transfer, with various ideas discussed.

In Press Physical Review E Rapid Communication (2014).

PACS numbers: 52.65.Kj, 47.27.ek, 52.35.Ra

On large length scales kinetic plasma effects can be neglected and magnetohydrodynamics (MHD) gives a good first order approximation to plasma evolution. The relevance of MHD turbulence ranges from industrial application, fusion research, solar physics (*e.g.* coronal heating) to astrophysics and cosmology, where it might leave detectable signatures in astrophysical processes [1] and even for the very early universe the possibility of a large-scale primordial magnetic field [2–5]. While there are many applications of MHD turbulence research in the above areas, some of the theoretical problems still remain open. Fundamental research in MHD turbulence consists of many active fields such as the amplification of a seed magnetic field by dynamo processes [6], different proposed models concerning the scaling of the energy spectra taking small-scale anisotropy into account [7], and MHD turbulence decay to name only a few.

Selective decay [8, 9], that is the decay of ideal quadratic invariants of MHD flows at different rates, dominates the nonlinear evolution of decaying turbulent MHD flows. It is related to the direction of spectral transfer of said ideal invariants. The magnetic helicity, which is one of the three ideal invariants of MHD flows (the other two being the total energy and the cross helicity), has been shown to influence the evolution of the magnetic field [11, 12] possibly through its reverse spectral transfer (RST) ¹ [13]. An understanding of the underlying mechanism of RST remains elusive, though much progress has been made.

In this paper we expand the numerical study of RST and its effects on MHD turbulence decay to ensemble-averaged data, which permits more reliable numerical exploration of the MHD equations compared to the sin-

gle realization studies done up to now. We also deconstruct the nonlinear MHD equations and identify some of the underpinnings of RST. Here we treat incompressible MHD turbulence only, and the magnetic Prandtl number is set to unity.

The incompressible decaying MHD equations are

$$\partial_t \mathbf{u} = -\frac{1}{\rho} \nabla P - (\mathbf{u} \cdot \nabla) \mathbf{u} + \frac{1}{\rho} (\nabla \times \mathbf{b}) \times \mathbf{b} + \nu \Delta \mathbf{u}, \quad (1)$$

$$\partial_t \mathbf{b} = (\mathbf{b} \cdot \nabla) \mathbf{u} - (\mathbf{u} \cdot \nabla) \mathbf{b} + \eta \Delta \mathbf{b}, \quad (2)$$

$$\nabla \cdot \mathbf{u} = 0 \quad \text{and} \quad \nabla \cdot \mathbf{b} = 0, \quad (3)$$

where \mathbf{u} denotes the velocity field, \mathbf{b} the magnetic induction expressed in Alfvén units, ν the kinematic viscosity, η the resistivity, P the pressure and $\rho = 1$ the density. Equations (1)–(3) are numerically solved in a cubic domain of length $L = 2\pi$ with periodic boundary conditions using a fully de-aliased pseudospectral MHD code, which we developed extending the hydrodynamic code of [14]. All simulations satisfy $k_{max} \eta_{mag,kin} \geq 1.26$, where $\eta_{mag,kin}$ are the Kolmogorov scales associated with the magnetic and velocity fields, respectively. We do not impose a background magnetic field, and both the initial magnetic and velocity fields are random Gaussian with zero mean, with initial magnetic and kinetic energy spectra $E_{mag,kin}(k) \sim k^4 \exp(-k^2/(2k_0)^2)$, unless otherwise specified. The peak wavenumber k_0 is varied for different simulations depending on the desired scale separation and resolution requirements. The initial relative magnetic helicity is $\rho_{mag}(k) = k H_{mag}(k)/2E_{mag}(k) = 1$, the initial cross helicity is negligible and the initial velocity field is non-helical, unless otherwise specified. The ratio between magnetic and kinetic energies $\Gamma(t) = E_{kin}(t)/E_{mag}(t)$ equals unity at $t = 0$, where $E_{mag,kin}(t) = \int dk E_{mag,kin}(k, t)$. All spectral quantities have been shell- and ensemble-averaged. Results have been obtained for a range of Reynolds numbers; the figures show data from the highest resolved simulations only. A summary of simulation details is shown in Table

* ab@ph.ed.ac.uk

† m.linkmann@ed.ac.uk

¹ The alternative terminology “inverse cascade” might be inaccurate as it implies spectral locality [10].

I, further details including benchmarking against results in the literature [15, 16] can be found in [17].

The numerous single realization studies of RST make it evident that it should also appear as a property in ensemble-averaged data, but this is the first analysis to adopt this procedure. In isotropic hydrodynamic turbulence it is pointed out in [18] that the direct cascade of kinetic energy is an ensemble-averaged concept and in [19] that a single realization could show energy transfer towards small wavenumbers, and it is the mean kinetic energy transfer that proceeds from low to high wavenumbers. At low k , the regime important for RST, shell averaging is not an optimal averaging method, since there is only a small number of points to average over. Furthermore, the modes in a given k -shell do not evolve independently from each other, as they become increasingly correlated by nonlinear mode coupling, whereas different realizations in an ensemble are statistically independent. It has also been noted that the actual measuring process in experimental studies of decaying turbulence results in an ensemble average [8].

Our ensemble-averaged results for $E_{mag}(k)$ and $H_{mag}(k)$ at different times are shown in Fig. 1 for run H9 in Table I, where the helicity spectra have been shifted for easier comparison. Error bars have been omitted to facilitate visual comparison between spectra at different times, but it should be noted that the measured spectra do not lie within the error of one another. The inset of Fig. 1 shows the flux of magnetic helicity $-\Pi_H(k) = \int_0^k dk' T_H(k')$, where $T_H(k')$ denotes the transfer spectrum of the magnetic helicity [9], at one and five initial large eddy turnover times t_0 in the very low k region. It is positive (as is $H_{mag}(k)$ at all times), which again indicates RST, but not constant. This indicates the absence of an inertial range, hence the observed RST here cannot be named a cascade. This is in accord with standard results in this wavenumber range; an inertial range is not expected at the very low k [10]. For visual purposes, we show a low R_λ result, which allows for higher scale separation at the low wavenumbers. Higher R_λ results showing an inertial range for the magnetic helicity in the higher k direct cascade region can be found in [17].

RST can also be studied through $E_{mag}(t)$ and $E_{kin}(t)$. Since RST sends magnetic energy from small length scales back to large length scales, where dissipation is smaller, $E_{mag}(t)$ should decay slower than $E_{kin}(t)$. There is agreement in the MHD literature that $E_{kin} \sim t^{-1}$ [5, 11, 20–22]. For $E_{mag} \sim t^{-n_E}$ in helical MHD turbulence decay there are conflicting results on the decay exponent n_E , with two asymptotic decay laws proposed. One model assumes equipartition of $E_{kin}(t)$ and $E_{mag}(t)$ during turbulence decay [11], leading to the asymptotic decay law $E_{mag}(t) \sim t^{-2/3}$. The second model proposes $E_{mag} \sim E_{tot}(t) \sim t^{-1/2}$ and has been derived in [11, 22] as an asymptotic decay law for the *total* energy with respect to late times in the decay when the decreasing ratio $\Gamma = E_{kin}/E_{mag}$ is small, thus not assuming

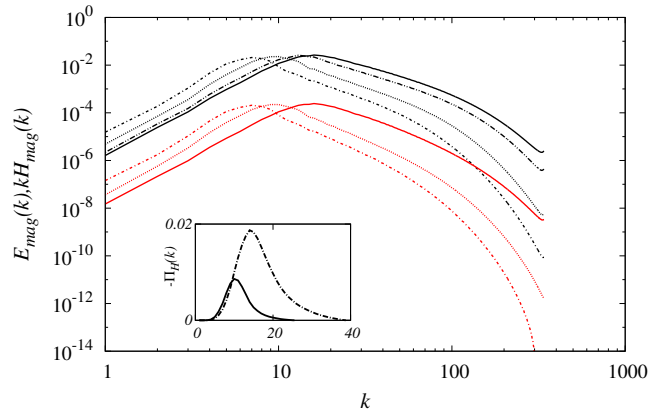


FIG. 1. (Color online) Magnetic energy and helicity spectra of run H9 showing reverse spectral transfer. The black (upper) lines refer to $E_{mag}(k)$, red (lower) lines to $kH_{mag}(k)$. Solid lines indicate one initial turnover time t_0 , dotted and dash-dotted lines refer to $2t_0$, $5t_0$ and $10t_0$. The inset shows the flux of magnetic helicity at t_0 and $5t_0$.

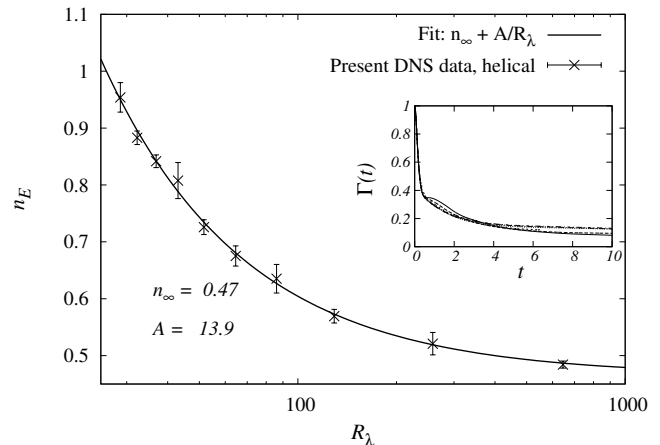


FIG. 2. Reynolds number dependence of decay exponents of $E_{mag}(t)$ for maximally helical initial magnetic fields. The inset shows the decay of $\Gamma(t)$ for runs H3-H11.

equipartition. Both decay laws have been observed to a good approximation for runs at specific Reynolds numbers [5, 11, 22, 23]. One case [24] studied a range of low Reynolds numbers and attempted an extrapolation which supported the second model.

Ensemble averaging permits a straightforward means to compute the statistical error on the measured quantity, here n_E , whereas with a single realization the only error one can obtain is the error on the fit. Furthermore, for high resolution simulations one usually assumes that the ensemble average can be replaced with the volume average of one realization. Since RST generates long-range correlations, different regions in phase space will eventually become statistically correlated and the volume average will not reflect this. We observed that the

energy spectra and the derived decay curves showed little deviations between realizations for $t < 7t_0$, while around $t \geq 7t_0$ the deviations became significant. As an example, for run H2 n_E varied from 0.81-0.96 between realizations if measured for $t > 7t_0$. Further details can be found in [17].

We measured n_E at for a $R_\lambda(0)$ -range of 28.69–645.47 using ensembles of typically 10 runs on up to 1032^3 grid points (see Table I), with our results in Fig. 2. The largest simulation H11 was run up to $t = 27t_0$, while the lower resolved runs reached $t = 64t_0$. As shown in the Figure, we find n_E has a $1/R_\lambda$ dependence. Extrapolating from this data to the infinite Reynolds number limit results in an asymptotic decay law $E_{mag}(t) \sim t^{-n_{E,\infty}}$ with $n_{E,\infty} = 0.47 \pm 0.03$. These results show that decay of magnetic energy in a helical system is slower than kinetic energy, thus supporting the presence of RST. Moreover, our asymptote is consistent with the second model mentioned above [11, 22] and is unambiguously not consistent with the first model. As can be seen in the inset of Fig. 2, the ratio $\Gamma(t) = E_{kin}(t)/E_{mag}(t)$ decreases over time. Our results also go further than [11, 22] as they yield finite Reynolds number results and a $1/R_\lambda$ dependence of n_E . A Reynolds number dependence of n_E consistent with $n_{E,\infty} = 1/2$ had been found before [24], albeit at much lower resolution using Reynolds numbers defined with respect to a lengthscale associated with the helicity. We also found that the evolution of the integral scale approaches $L_{mag}(t) \sim t^{1/2}$ (not shown). This is consistent with the approximate conservation of magnetic helicity at large magnetic Reynolds number, since $H_{mag}(t) \sim E_{mag}(t)L_{mag}(t)$ [9].

For the nonhelical case we have done a small analysis in response to [25] for ensembles of 10 runs on up to 512^3 grid points, resulting in exponents consistent with $E_{mag}(t) \sim t^{-1}$, in agreement with [4, 5, 20] and the theoretical analysis by Campanelli [21]. Since the decay exponents of $E_{kin}(t)$ and $E_{mag}(t)$ coincide for a nonhelical magnetic system, if one field shows RST so should the other, provided RST is large enough to influence the time evolution of the system. Brandenburg *et al.* [25] recently reported RST of magnetic and kinetic energies from a single realization run of an initially nonhelical magnetic system on 2304^3 grid points. Our ensemble of runs shows similar behavior for the magnetic energy.

To further investigate RSTs we made an *ad hoc* modification of the momentum equation (1) by omitting the Lorentz force $(\nabla \times \mathbf{b}) \times \mathbf{b}$, which decouples the velocity field from the magnetic field. This approach clearly does not lead to a faithful representation of MHD, since the decoupled fluid-magnetic field system ceases to be energetically closed. Its purpose is to serve as a diagnostic tool to unravel the complicated nonlinear set of equations to allow understanding the mathematical properties of the induction equation (2) as a linear partial differential equation. In particular, one can test if RST is among those mathematical properties.

The logic behind this modification can be viewed in

another way. One can solve the full MHD equations and store the $\mathbf{u}(\mathbf{x}, t)$ solution. One can imagine now doing this slightly differently by solving just the induction equation with the same initial conditions using the above stored $\mathbf{u}(\mathbf{x}, t)$ function. In both cases one obtains exactly the same solution for $\mathbf{b}(\mathbf{x}, t)$. However in the second case it was through the solution of a linear partial differential equation with variable coefficients, here given by $\mathbf{u}(\mathbf{x}, t)$. The step made here is to provide an alternative viewpoint, that is the entire problem of RST can be analyzed through solving a linear partial differential equation with variable coefficients. This is still a hard problem, but now linear and thus tractable. One way forward is to dismiss the MHD equations and study the induction equation in isolation with different external \mathbf{u} -fields, as a means to probe this equation for features that produce RST. That is what we did here with perhaps the most obvious initial example of an independently evolving turbulent \mathbf{u} -field, and as will be shown below, have found even in that case, the induction equation leads to RST.

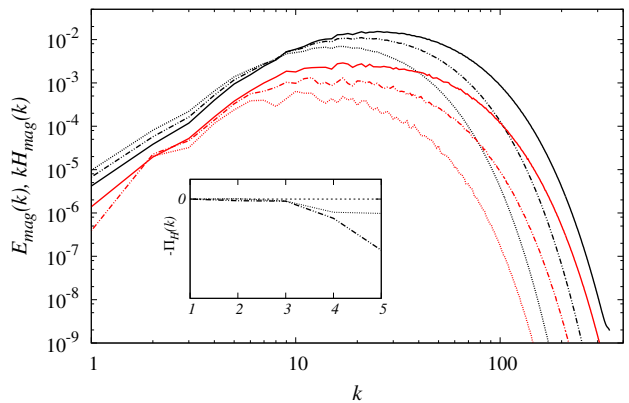


FIG. 3. (Color online) Magnetic energy spectra showing reverse spectral transfer for the decoupled system (run Hd5). Note the absence of RST for the magnetic helicity. The black (upper) lines refer to $E_{mag}(k, t)$, red (lower) lines to $kH_{mag}(k, t)$, solid lines are earlier in time than dotted lines. The inset shows the flux of magnetic helicity.

We have conducted simulations for this decoupled system on up to 1032^3 grid points with our results shown in Fig. 3 for an ensemble of 10 runs. As seen in this Figure, there is a RST of magnetic energy, which is interesting since it emerges from a linear equation. To diminish the possibility of a finite-size effect, we set the peak of the initial spectra relatively high, *e.g.* in Fig. 3 $k_0 = 23$. Moreover, we have done several tests [17] to verify this linear RST, such as reproducing the same effect in slightly compressible MHD using the PENCIL CODE [26].

Interestingly, we do not find RST of magnetic helicity in these simulations. The reverse transfer of $E_{mag}(k, t)$ is usually thought to be driven by the reverse transfer of $H_{mag}(k, t)$ by virtue of the realizability condition

$|H_{mag}(k, t)| \leq 2E_{mag}(k, t)/k$ [9]. Our results show that RST of magnetic energy is possible without RST of magnetic helicity, despite the magnetic field being initially maximally helical. Although some realizations showed RST of $H_{mag}(k, t)$ at $k = 1$ and there appears to be a hint of RST at $k = 2$, the ensemble average strongly supports the absence of RST of $H_{mag}(k, t)$. The data point at $k = 2$ lies within the error of the ensemble averaged data at earlier time. The flux of magnetic helicity is shown in the inset of Fig. 3 to be negative at low k , thus indicating the absence of RST, as opposed to the coupled case shown in Fig. 1, where it is positive at low k .

As the velocity field is not influenced by the magnetic field in this decoupled system and is initially non-helical for the results in Fig. 3, effects of kinetic helicity could not influence the evolution of the magnetic field. However having decoupled these two equations, it permits us to cleanly test the influence that kinetic helicity can have on the magnetic system. In Fig. 4 our initial \mathbf{u} - and \mathbf{b} -

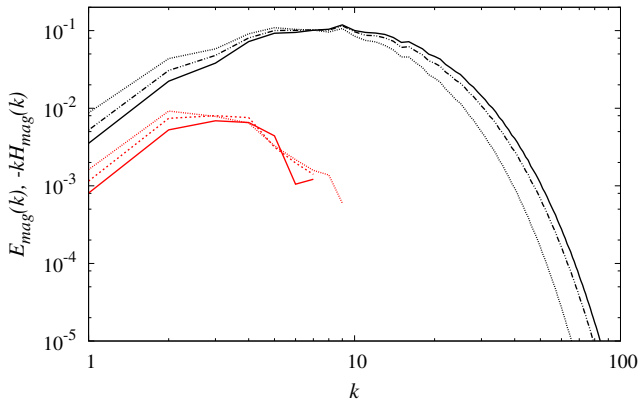


FIG. 4. (Color online) Magnetic energy and helicity spectra for the decoupled case Hd4 showing RST for an initially helical velocity field. The black (upper) lines refer to $E_{mag}(k, t)$, red (lower) lines to $-kH_{mag}(k, t)$, solid lines are earlier in time than dotted lines. Since $H_{mag}(k, t)$ is positive at larger k , it does not show on logarithmic scales.

fields were set to be maximally helical in the same direction and now we observe RST of both magnetic energy and helicity. In particular, this simulation was started with $H_{mag}(k) > 0$ for all $k > 0$, and we found the magnetic helicity to increase at large wavenumbers while it decreased at low wavenumbers, eventually changing sign. The now negative magnetic helicity is subsequently transferred to lower k . This suggests that RST of magnetic helicity relies on the presence of kinetic helicity, which hints at a connection between large-scale dynamo action and RST of $H_{mag}(k, t)$.

We also examined in our decoupled equations the case of an initially nonhelical magnetic field. Two cases were investigated here, one with $E_{mag}(k, 0) = E_{kin}(k, 0) \sim k^4$ at low k and one with $E_{kin}(k, 0) \sim k^2$ while $E_{mag}(k, 0) \sim$

| Run id | N^3 | $R_\lambda(0)$ | $10^3\eta$ | k_0 | # | t_{max} |
|---------|-------------------|----------------|------------|-------|----|-----------|
| H1-8,10 | 128^3 - 528^3 | 28.69-258.19 | 9-1 | 5-15 | 10 | 50 |
| H9 | 1024^3 | 74.84 | 0.75 | 23 | 10 | 6 |
| H11 | 1032^3 | 645.47 | 0.4 | 5 | 5 | 22 |
| NH1-6 | 128^3 - 512^3 | 28.69-172.13 | 9-1.5 | 5 | 10 | 10-50 |
| Hd1-4 | 256^3 - 528^3 | 43.03-57.38 | 6-4.5 | 5 | 10 | 5 |
| Hd5 | 1032^3 | 28.06 | 2 | 23 | 10 | 2 |
| NHd1-3 | 256^3 - 512^3 | 43.03-57.38 | 6-4.5 | 5 | 10 | 5 |

TABLE I. Specifications of simulations. H and NH refer to initially helical and non-helical magnetic fields, respectively. The additional letter d refers to the decoupled system, η denotes the magnetic resistivity, k_0 the peak wavenumber of the initial energy spectra and # the ensemble size.

k^4 at low k as in [25]. We found RST in both cases, more pronounced in the second than in the first case. These results further support the findings in [25, 27] on nonhelical RST, now also for our linear RST.

A plausible explanation of these observations would be that RST of magnetic energy has two components, a dominant (non-linear) one due to the reverse transfer of magnetic helicity and a residual (linear) one which is slightly augmented by the presence of magnetic helicity. Our numerical results show that coupling between helical modes has an impact on RST, especially if the coupling includes helical \mathbf{u} -modes. For initially helical \mathbf{u} -fields we also saw that coupling between positively helical \mathbf{b} - and \mathbf{u} -modes led to a positively helical magnetic field becoming negatively helical. Decomposing both fields into helical modes to study the mode couplings might lead to further insight.

In order to understand the physical nature of RST, an analytic study of the induction equation as a linear partial differential equation in this decoupled system might lead to further insight and can serve to get a step further towards the full nonlinear problem. The induction equation can be further studied using classical techniques such as Green's functions and integral transforms. One could further dissect it by retaining one of the transfer terms only. If the advective term $(\mathbf{u} \cdot \nabla)\mathbf{b}$ is retained, we obtain an advection-diffusion equation, which has been extensively studied in the literature. The nature of the linear RST would be different depending on which of the transfer terms produces it, and this could inspire models to be put forward that highlight physical processes responsible for the full nonlinear RST, which is analytically intractable. In the case of the kinetic source term $(\mathbf{b} \cdot \nabla)\mathbf{u}$, RST would be a transfer of *kinetic* to magnetic energy, while in the case of the advective term the transfer would be of magnetic energy only.

In summary, this paper presented the first ensemble-averaged measurements of reverse spectral transfer of magnetic energy and helicity, which show that these forms of transfer are statistical properties of the MHD equations. Our analysis showed that at early times single realization measurements are sufficient to replicate the

properties of the ensemble average, while at later times in the decay the ensemble average becomes a must, as we observed larger deviations between realizations. Turbulence decay is influenced by reverse spectral transfer; in the helical case we observed a Reynolds number dependence of the decay exponent $n_E = n_\infty + A/R_\lambda$ with $n_\infty \simeq 1/2$ and $A = 13.9 \pm 0.8$. The reverse transfers of magnetic energy and magnetic helicity were further investigated in a simplified system, which decoupled the evolution of the velocity field from the magnetic field.

The magnetic helicity shows no reverse transfer in this system, and a new aspect of reverse transfer of magnetic energy was found, which is linear in nature and thus amenable to further mathematical analysis.

We thank David McComb for helpful advice on turbulence theory and numerical simulations. This work has made use of the resources provided by HECToR and ARCHER [28], made available through ECDF [29]. AB acknowledges funding from STFC, and ML is supported by EPSRC.

-
- [1] A. Beresnyak, Phys. Rev. Lett. **108**, 035002 (2012). J. Cho, A. Lazarian, and E. T. Vishniac, in *Turbulence and Magnetic Fields in Astrophysics* (Springer, Berlin Heidelberg, 2003), pp. 56–98. A. A. Schekochihin and S. C. Cowley, in *Magnetohydrodynamics-Historical Evolution and Trends* (Springer, Berlin, 2007), pp. 85–115.
 - [2] A. Brandenburg, K. Enqvist, and P. Olesen, Phys. Rev. D **54**, 1291 (1996).
 - [3] D. T. Son, Phys. Rev. D **59**, 063008 (1999).
 - [4] A. G. Tevzadze, L. Kisslinger, A. Brandenburg, and T. Kahniashvili, Astrophys. J. **759**, 54 (2012).
 - [5] T. Kahniashvili, A. G. Tevzadze, A. Brandenburg, and A. Neronov, Phys. Rev. D **87**, 083007 (2013).
 - [6] S. M. Tobias, F. Cattaneo, and S. Boldyrev, in *Ten Chapters in Turbulence* (Cambridge University Press, 2013), pp. 351–405. J. Cho and E. T. Vishniac, Astrophys. J. **538**, 217 (2000). E. T. Vishniac and J. Cho, Astrophys. J. **550**, 752 (2001).
 - [7] R. S. Iroshnikov, Sov. Astron. **7**, 566 (1963). R. H. Kraichnan, Phys. Fluids **8**, 1365 (1965). P. Goldreich and S. Sridhar, Astrophys. J. **438**, 763 (1995).
 - [8] P. D. Mininni and A. Pouquet, Phys. Rev. E **87**, 033002 (2013).
 - [9] D. Biskamp, *Nonlinear Magnetohydrodynamics*. (Cambridge University Press, 1993), 1st ed.
 - [10] W. C. Müller, S. K. Malapaka, and A. Busse, Phys. Rev. E **85**, 015302 (2012).
 - [11] D. Biskamp and W.-C. Müller, Phys. Rev. Lett. **83**, 2195 (1999).
 - [12] W.-C. Müller and D. Biskamp, Phys. Rev. Lett. **84**, 03475 (2000).
 - [13] A. Pouquet, U. Frisch, and J. Léorat, J. Fluid Mech. **77**, 321 (1976).
 - [14] S. R. Yoffe, Ph.D. thesis, University of Edinburgh (2012), <http://arxiv.org/pdf/1306.3408v1.pdf>.
 - [15] P. D. Mininni, A. G. Pouquet, and D. C. Montgomery, Phys. Rev. Lett. **97**, 244503 (2006).
 - [16] J. A. Morales, M. Leroy, W. J. T. Bos, and K. Schneider, J. Comp. Phys. **274**, 64 (2014).
 - [17] Supplemental Material.
 - [18] P. Sagaut and C. Cambon, *Homogeneous Turbulence Dynamics* (Cambridge University Press, Cambridge, p. 95, 2008).
 - [19] W. D. McComb, *Homogeneous, Isotropic Turbulence: Phenomenology, Renormalization and Statistical Closures* (Oxford University Press, p. 82, 2014).
 - [20] M. Christensson, M. Hindmarsh, and A. Brandenburg, Phys. Rev. E **64**, 056405 (2001).
 - [21] L. Campanelli, Phys. Rev. D **70**, 083009 (2004).
 - [22] D. Biskamp and W.-C. Müller, Phys. Plasma **7**, 4889 (2000).
 - [23] S. K. Malapaka and W.-C. Müller, Astrophys. J. **778** (2013).
 - [24] M. Christensson, M. Hindmarsh, and A. Brandenburg, Astron. Nachr. **326**, 393 (2005).
 - [25] A. Brandenburg, T. Kahniashvili, and A. G. Tevzadze, <http://arxiv.org/abs/1404.2238> (2014).
 - [26] <http://pencil-code.googlecode.com/>.
 - [27] J. Zrake, <http://arxiv.org/pdf/1407.5626v1.pdf> (2014).
 - [28] <http://www.hector.ac.uk/>. <http://www.archer.ac.uk/>.
 - [29] <http://www.ecdf.ed.ac.uk/>.

Supplemental Material for "Magnetic helicity and the evolution of decaying magnetohydrodynamic turbulence"

Arjun Berera and Moritz Linkmann

SUPA, School of Physics and Astronomy, University of Edinburgh, UK

In this supplemental material we provide details of our investigation of reverse spectral transfers in magnetohydrodynamic turbulence, such as verification of our code and further tests of our results.

I. INTRODUCTION

In the paper [1] we conducted direct numerical simulations (DNS) of incompressible magnetohydrodynamic (MHD) turbulence without an imposed guide field. The MHD equations for incompressible flow are

$$\partial_t \mathbf{u} = -\frac{1}{\rho} \nabla P - (\mathbf{u} \cdot \nabla) \mathbf{u} + \frac{1}{\rho} (\nabla \times \mathbf{b}) \times \mathbf{b} + \nu \Delta \mathbf{u} , \quad (1)$$

$$\partial_t \mathbf{b} = (\mathbf{b} \cdot \nabla) \mathbf{u} - (\mathbf{u} \cdot \nabla) \mathbf{b} + \eta \Delta \mathbf{b} , \quad (2)$$

$$\nabla \cdot \mathbf{u} = 0 \quad \text{and} \quad \nabla \cdot \mathbf{b} = 0 , \quad (3)$$

where \mathbf{u} denotes the velocity field, \mathbf{b} the magnetic induction expressed in Alfvén units, ν the kinematic viscosity, η the resistivity, P the pressure and $\rho = 1$ the density.

We presented ensemble averaged data showing reverse spectral transfer (RST) of magnetic helicity and measured decay exponents for initially maximally helical magnetic fields. In a particular set of simulations we decoupled the momentum equation (1) from the induction equation (2) and showed that the inverse cascade of magnetic energy persists, while the reverse spectral transfer of magnetic helicity disappears in the decoupled system, provided the initial velocity field was nonhelical.

Details of our simulations can be found in Table I, where we specify values for Reynolds numbers, resolution, diffusivities, runtime t_{max} , ensemble size and wavenumber k_0 at which we set the peaks of the initial spectra.

II. VERIFICATION OF DNS CODE

The 3D Orszag-Tang vortex was used for comparison against results by Mininni, Pouquet and Montgomery [2] and Morales, Leroy, Bos and Schneider [3]. The initial conditions are

$$\begin{aligned} \mathbf{u} &= (-2 \sin y, \ 2 \sin x, \ 0) , \\ \mathbf{b} &= \beta(-2 \sin 2y + \sin z, \ 2 \sin x + \sin z, \ \sin x + \sin y) , \end{aligned} \quad (4)$$

where $\beta = 0.8$ has been chosen according to [2, 3]. We calculate the total dissipation

$$\varepsilon_{tot}(t) = \nu \langle \omega^2 \rangle + \eta \langle \mathbf{j}^2 \rangle , \quad (5)$$

and the maximum of the current density in real space $\max |\mathbf{j}|$. We used the same number of grid points and diffusivities as [3], that is $\nu = \eta = 0.01$ on 64^3 points, $\nu = \eta = 0.005$ on 128^3 points and $\nu = \eta = 0.001$ on 256^3 points. Our results are in agreement with both above mentioned sources. The maximum of the current density shows Reynolds number independent exponential growth until $t = 0.4$, in agreement with Morales *et al.*, while Mininni *et al.* observe exponential growth up to $t = 0.6$. After this initial period we observe algebraic growth $\sim t^3$ in agreement with

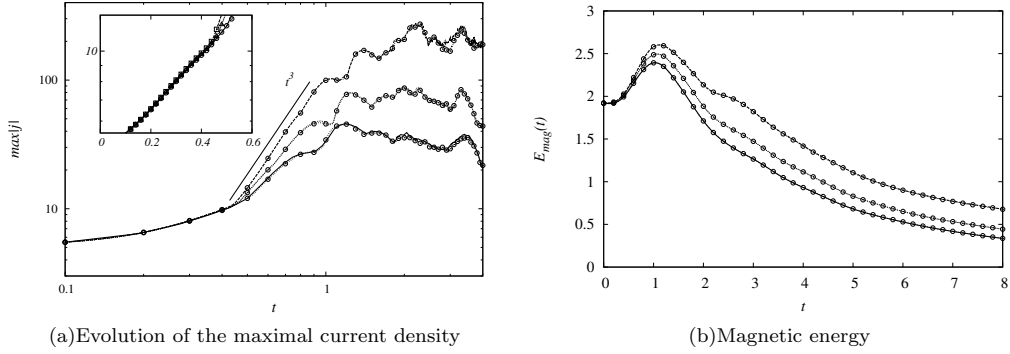


FIG. 1. Comparison to Morales *et al.* The symbols refer to our DNS, the lines to DNS by Morales *et al.*

both sources. With increasing Reynolds number the temporal maxima of $\max|\mathbf{j}|$ are achieved at later times, also in agreement with both sources. Our data shows very good agreement to a dataset obtained from Morales *et al.* [3], see Fig. 1.

III. INERTIAL RANGE PROPERTIES FOR THE FULL MHD EQUATIONS.

Figure 2 shows magnetic helicity, magnetic energy and kinetic energy spectra shortly after the onset of power-law decay (that is, at $t = 1.3t_0$) for the largest Reynolds number run H11. The magnetic helicity spectra have been multiplied by the wavenumber k for dimensional reasons, and have been shifted downwards in the figure to facilitate visual analysis. The inset shows constancy of helicity flux $\Pi_H(k)$ for the wavenumber interval $21 \leq k \leq 33$, indicating an inertial range for the magnetic helicity in the direct cascade region. It can be seen in the figure that power-law scaling of $H_{mag}(k)$ extends over a larger interval, showing the scaling $H_{mag}(k) \sim k^{-3.6}$, which is in agreement with recent results on decaying 3D MHD turbulence [4]. The flux is k -dependent in the reverse spectral transfer region, as shown in the paper in the inset of Fig. 1 for the lower R_λ -run H9 and here in the inset of Fig. 5(a) for run H4a. This is also in agreement with [4], who report the same behavior. Our simulations support Kolmogorov scaling for the magnetic field as indicated by the bar parallel to $E_{mag}(k)$.

IV. EVOLUTION OF THE LOW WAVENUMBER FORM OF KINETIC ENERGY SPECTRA FOR THE FULL MHD EQUATIONS.

Figure 3 shows kinetic and magnetic energy spectra on logarithmic scales at different times during the decay for run H9, which is the run with the largest scale separation. Note that the slope of $E_{kin}(k)$ becomes flatter over time while the slope of $E_{mag}(t)$ remains the same, that is $E_{mag}(k) \sim k^4$ at small k prevails, as indicated the diagonal line superimposed above $E_{mag}(k)$ in the low wavenumber region. The slope of $E_{kin}(k)$ does *not* change from k^4 to k^2 , instead it continues to flatten over time.

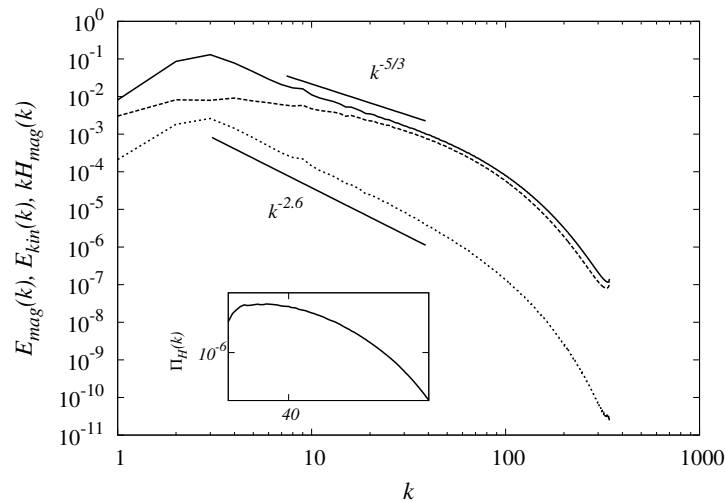


FIG. 2. Spectra for the largest Reynolds number run (H11). The solid line shows $E_{mag}(k)$, the middle dashed line shows $E_{kin}(k)$ and the bottom dotted line shows $kH_{mag}(k)$, which has been shifted for easier comparison. The inset shows the flux of $H_{mag}(k)$, which is constant in the higher k region, indicating an inertial range. The straight lines indicate scaling regions for $E_{mag}(k) \sim k^{-5/3}$ and $kH_{mag}(k) \sim k^{-2.6}$, which results in $H_{mag}(k) \sim k^{-3.6}$.

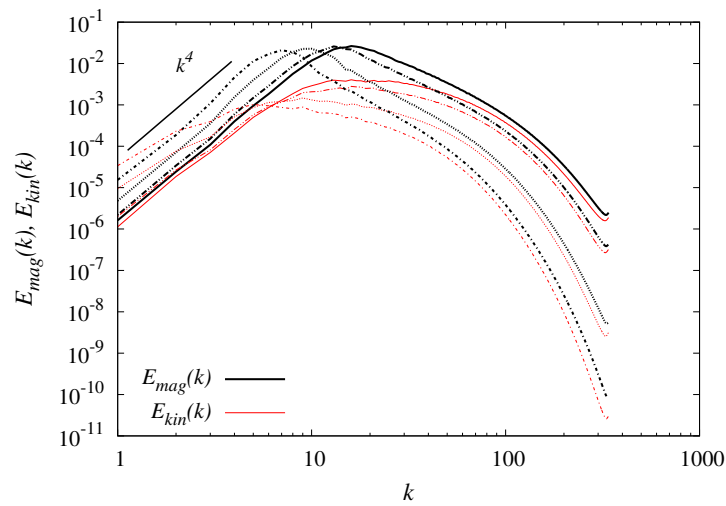


FIG. 3. (Color online) Evolution of kinetic (thin red (grey) lines) and magnetic (thick black lines) energy spectra over time for run H9. Note how the slope of $E_{kin}(k)$ flattens with time, while the slope of $E_{mag}(k)$ remains unchanged.

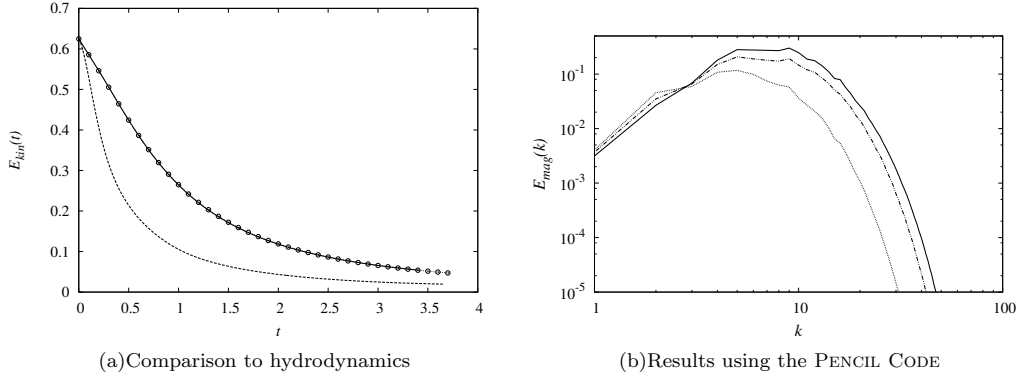


FIG. 4. (a) The solid line shows $E_{kin}(t)$ from a hydrodynamic run, the symbols shows $E_{kin}(t)$ from a simulation where the momentum equation was decoupled from the induction equation, and the dashed line shows $E_{kin}(t)$ of a full MHD run. The evolution of $E_{kin}(t)$ coincides for the hydrodynamic run and the simulation of the decoupled case, showing that in the decoupled case the velocity field evolves independently of the magnetic field, as expected. (b) Linear RST of magnetic energy using the PENCIL CODE on 128^3 grid points.

V. FURTHER TESTS OF LINEAR RST

We have conducted further tests in order to validate the linear RST found in our simulations. The velocity field should evolve as in hydrodynamic turbulence if the Lorentz force term is omitted from the momentum equation. We have tested that this is the case, see Fig. 4(a), this test clearly shows that the velocity field evolves independently from the magnetic field. The linear RST of magnetic energy was also found for slightly compressible MHD using the PENCIL CODE [5]. Figure 4(b) shows that after removing the Lorentz force term in the momentum equation in the PENCIL CODE we still observe RST of magnetic energy.

Results for the linear RST of magnetic energy were found in simulations using 256^3 up to 1032^3 collocation points, but only the highest resolved results with the largest scale separation are included in the paper [1]. Figure 5(b) shows results from simulations using 512^3 collocation points (Hd3), where the peaks of the initial spectra had been set at $k_0 = 5$. The linear RST is still visible, but concentrated at the very lowest wavenumbers. In contrast, the simulation results shown in the paper are obtained by setting the peaks of the initial spectra at $k_0 = 23$, and RST can be seen up to $k = 7$ in Fig. 3(a) of the paper. Figure 5(b) also shows that RST is absent for the magnetic helicity, as there is no increase of $H_{mag}(k)$ at the low wavenumbers and the flux of magnetic helicity is negative. For comparison, the coupled case shows RST for both $H_{mag}(k)$ and $E_{mag}(k)$ as can be seen in Fig. 5(a), where the inset shows positive flux of kinetic helicity in the low k region.

Figure 6 shows that our simulations have converged for the time-step chosen. We do not see differences in the magnetic energy spectra and the magnetic energy as we reduce the time-step, results are shown for 256^3 grid points.

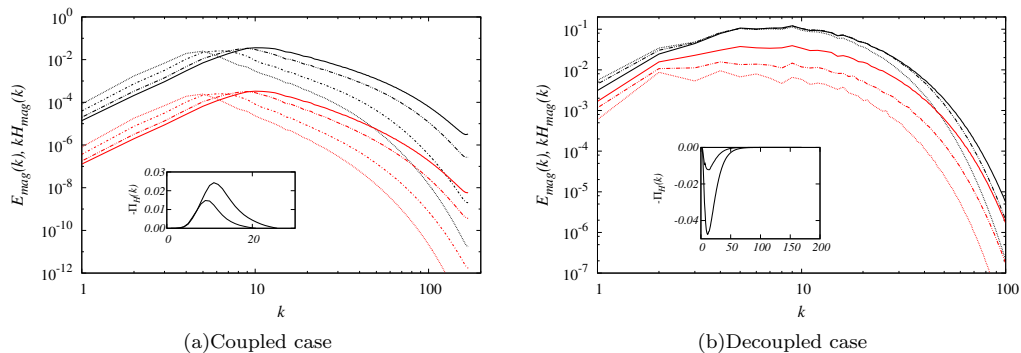


FIG. 5. (a) (Color online) Magnetic energy and helicity spectra showing reverse spectral transfer for a run on 512^3 grid points (H4a). The black (upper) lines refer to $E_{mag}(k)$, red (lower) lines refer to $H_{mag}(k)$. Solid lines indicate one initial large eddy turnover time, dotted and dash-dotted lines refer to 2, 5 and 10 turnover times. The inset shows the flux of magnetic helicity at one and two turnover times. (b) Magnetic energy and helicity spectra for the decoupled case on 512^3 grid points (Hd3). Upper (black) lines refer to $E_{mag}(k)$, lower (red) lines to $H_{mag}(k)$. The inset shows the flux of magnetic helicity.

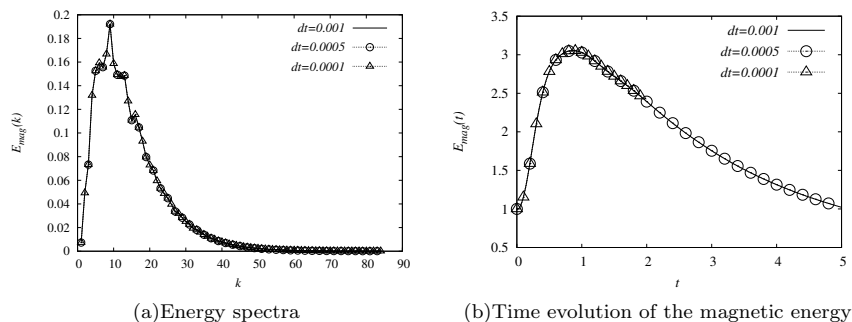


FIG. 6. (a) Results for magnetic energy spectra from simulations run at different time-steps on 256^3 grid points. The spectra obtained from simulations using different time-steps coincide. (b) The evolution for the magnetic energy is the same for simulations using different time-steps.

VI. IMPORTANCE OF ENSEMBLE AVERAGING

A. Decay exponents

Figure 7 illustrates the importance of ensemble averaging for the measurement of the decay exponent n_E , showing all realizations of H2 and the ensemble average. It can clearly be seen how the decay exponents for single realizations differ at later times, and how they deviate from the exponent measured at early times. By contrast, the ensemble average follows the same straight line for all times after the onset of power-law decay. Similarly, a recent study of 2D hydrodynamic turbulence [6] using ensemble averaging showed a significant spread in the evolution of the integral

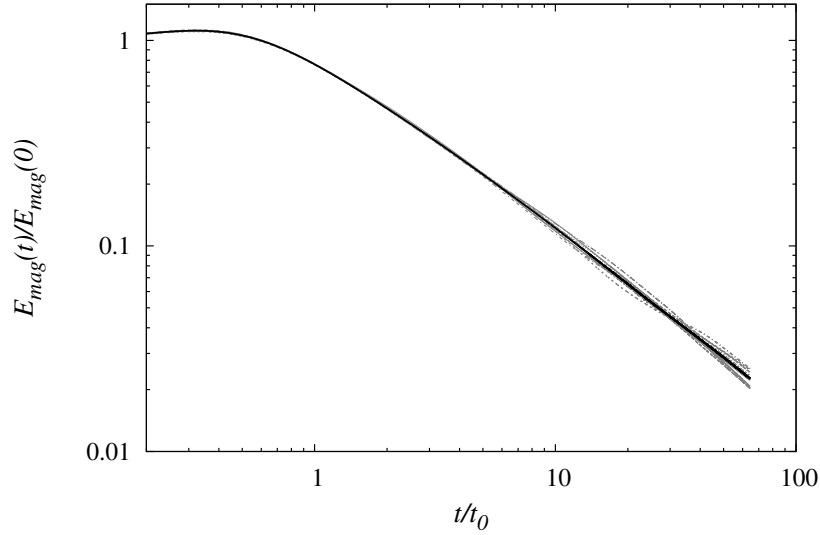


FIG. 7. Deviation of realizations (grey lines) from the ensemble average (black line) of run H2. Note that there is a clearly visible spread between realizations for $t/t_0 \geq 7$.

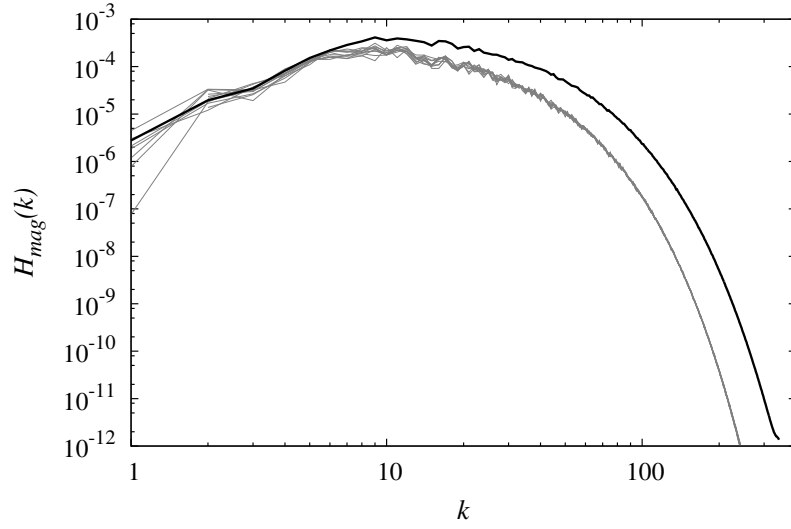
scale for different realizations and a somewhat less pronounced spread in the total energy decay curves (see their Fig. 3). The decay exponent n_E measured from individual realizations of H2 can range from 0.81-0.96 for $t > 7t_0$, where t_0 denotes the initial large eddy turnover time.

B. Magnetic helicity for the decoupled case

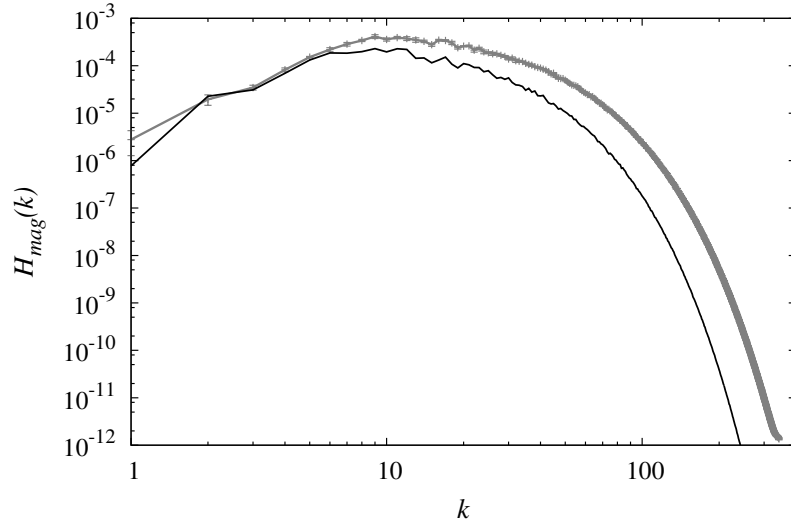
As mentioned in the paper [1], some realizations of Hd5 appeared to show RST, but the ensemble average did not confirm this. As can be seen in Fig. 8(a), the error on the ensemble averaged helicity spectrum is large at $k = 1$. Some realizations clearly show RST, some do not and some realizations show negative helicity at $k = 1$, which is why the value does not appear on a logarithmic scale.

Taking data from one realization only could have lead to erroneous results, claiming that either $H_{mag}(k)$ does show reverse spectral transfer, or that $H_{mag}(k)$ becomes negative at $k = 1$. The ensemble averaged result shows that neither is the case. For $k = 2$ there appears to be a hint of RST, but as can be seen in Fig. 8(b) the helicity spectrum at later time lies within the error of the helicity spectrum at earlier time.

We would like to thank Jorge Morales for kindly providing us with a dataset of simulation results using the Orszag-Tang vortex as initial condition.



(a) Helicity spectra of all realizations of the ensemble Hd5



(b) Ensemble averaged helicity spectra for run Hd5

FIG. 8. (a) The black line shows the ensemble average of $H_{mag}(k)$, the grey lines show $H_{mag}(k)$ for all realizations of run Hd5 at later time. Note the large deviations between realizations at low k . (b) The black line shows the ensemble average over the realizations in (a). What appears as a hint of RST at $k = 2$ lies within the error of the ensemble average at earlier time (grey line).

| Run id | N^3 | $k_{max}\eta_{mag}$ | $R_\lambda(0)$ | η | k_0 | # | t_{max}/s |
|--------|----------|---------------------|----------------|---------|-------|----|-------------|
| H1 | 128^3 | 1.30 | 28.69 | 0.009 | 5 | 10 | 50 |
| H2 | 256^3 | 2.42 | 32.27 | 0.008 | 5 | 10 | 50 |
| H3 | 256^3 | 2.18 | 36.88 | 0.007 | 5 | 10 | 50 |
| H4 | 256^3 | 2.08 | 43.03 | 0.006 | 5 | 10 | 50 |
| H5 | 256^3 | 1.80 | 51.64 | 0.005 | 5 | 10 | 50 |
| H6 | 256^3 | 1.59 | 64.55 | 0.004 | 5 | 10 | 50 |
| H7 | 256^3 | 1.30 | 86.06 | 0.0031 | 5 | 10 | 50 |
| H4a | 512^3 | 1.38 | 43.03 | 0.002 | 15 | 10 | 48 |
| H8 | 512^3 | 2.01 | 129.09 | 0.002 | 5 | 10 | 7 |
| H9 | 1024^3 | 1.38 | 74.84 | 0.00075 | 23 | 10 | 6 |
| H10 | 528^3 | 1.31 | 258.19 | 0.001 | 5 | 10 | 50 |
| H11 | 1032^3 | 1.38 | 645.47 | 0.0004 | 5 | 5 | 12 |
| NH1 | 128^3 | 1.29 | 28.69 | 0.009 | 5 | 10 | 50 |
| NH2 | 256^3 | 1.51 | 64.55 | 0.004 | 5 | 10 | 10 |
| NH3 | 256^3 | 1.26 | 86.06 | 0.003 | 5 | 10 | 12 |
| NH4 | 512^3 | 1.43 | 129.09 | 0.002 | 5 | 10 | 10 |
| NH5 | 512^3 | 1.30 | 172.13 | 0.0015 | 5 | 10 | 7 |
| Hd1 | 256^3 | 1.26 | 43.03 | 0.006 | 5 | 10 | 5 |
| Hd2 | 256^3 | 1.26 | 43.03 | 0.006 | 5 | 10 | 5 |
| Hd3 | 512^3 | 1.88 | 57.38 | 0.0045 | 5 | 10 | 5 |
| Hd4 | 528^3 | 1.95 | 57.38 | 0.0045 | 5 | 10 | 5 |
| Hd5 | 1032^3 | 1.39 | 28.06 | 0.001 | 23 | 10 | 2 |
| NHd1 | 256^3 | 1.26 | 43.03 | 0.006 | 5 | 10 | 5 |
| NHd2 | 256^3 | 1.26 | 43.03 | 0.006 | 5 | 10 | 5 |
| NHd3 | 512^3 | 1.88 | 57.38 | 0.0045 | 5 | 10 | 5 |

TABLE I. Specifications of simulations. H refers to an initially helical magnetic field, NH to an initially non-helical magnetic field. The additional letter d refers to the decoupled system, $R_\lambda(0)$ denotes the initial Taylor-scale Reynolds number, η the magnetic resistivity, k_0 the peak wavenumber of the initial energy spectra, k_{max} the largest resolved wavenumber, η_{mag} the Kolmogorov microscale associated with the magnetic field, # the ensemble size and t_{max} the run time. The run NHd2 was started from initial spectra following k^2 at low wavenumbers k , and runs Hd2 and Hd4 were started using a maximally helical initial velocity field.

-
- [1] A. Berera and M. F. Linkmann, (2014).
 - [2] P. D. Mininni, A. G. Pouquet, and D. C. Montgomery, Phys. Rev. Lett., **97**, 244503 (2006).
 - [3] J. A. Morales, M. Leroy, W. J. T. Bos, and K. Schneider, J. Comp. Phys., **274**, 64 (2014).
 - [4] W. C. Müller, S. K. Malapaka, and A. Busse, Phys. Rev. E, **85**, 015302 (2012).
 - [5] <http://pencil-code.googlecode.com/>.
 - [6] P. D. Mininni and A. Pouquet, Phys. Rev. E, **87**, 033002 (2013).